

Modeling Mercury Capture within ESPs: Continuing Development and Validation

Herek L. Clack

(Department of Mechanical, Materials and Aerospace Engineering, Illinois Institute of Technology
10 West 32nd Street, Chicago, Illinois 60616, USA)

Abstract: Efforts to reduce anthropogenic mercury emissions worldwide have recently focused on a variety of sources, including mercury emitted during coal combustion. Toward that end, much research has been ongoing seeking to develop new processes for reducing coal combustion mercury emissions. Among air pollution control processes that can be applied to coal-fired boilers, electrostatic precipitators (ESPs) are by far the most common, both on a global scale and among the principle countries of India, China, and the USA that burn coal for electric power generation. A previously reported theoretical model of in-flight mercury capture within ESPs is herein validated against data from a number of full-scale tests of activated carbon injection for mercury emissions control, resulting in the first validated model of mercury capture within ESPs. By using the established particle size distribution of the activated carbon and actual or estimated values of its equilibrium mercury adsorption capacity, the incremental reduction in mercury concentration across each ESP can be predicted and compared to experimental results. Because the model does not incorporate kinetics associated with gas-phase mercury transformation or surface adsorption, the model predictions represent the mass-transfer-limited performance. Comparing field data to model results reveals many facilities performing at or near the predicted mass-transfer-limited maximum, particularly at low rates of sorbent injection. Where agreement is poor between field data and model predictions, additional chemical or physical phenomena may be responsible for reducing mercury removal efficiencies.

Keywords: mercury capture, ESP, model prediction, sorbent injection

1 INTRODUCTION

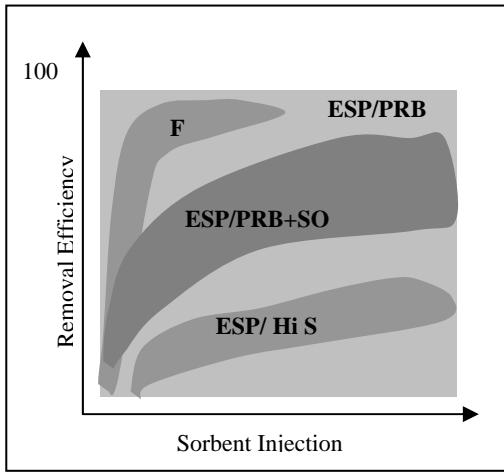
In anticipation of regulations to reduce mercury emissions from coal-fired power plants (CFPPs), the U.S. Department of Energy National Energy Technology Laboratory (DOE-NETL), in conjunction with a variety of funding partners, has invested over \$80M over 10 years in conducting several dozen pilot- and full-scale tests of mercury emissions control technologies for CFPPs [1]. The overarching goal of these tests has been to demonstrate at full-scale the effectiveness of technologies that are ready for full-scale testing, one of which is activated carbon injection (ACI) and injection of other sorbents. Results have revealed wide variability between different sites in mercury removal efficiency. Much of this variability is believed to result from interferences from other flue gas constituents and differences in the physical configurations of the CFPP sites. By grouping full-scale ACI test results by their CFPP site characteristics and type of coal burned, the data tend to cluster in “bands”, a simplified schematic of which is shown in Fig. 1. Presentation of the data in this way has been a common means of conveying current, demonstrated mercury emissions control performance for various configurations. However, despite the grouping into these performance bands, certain combinations of facility characteristics and coal type have shown substantial variability in mercury emissions control performance. In general, ACI upstream of a fabric filter has been shown to attain the highest mercury removal efficiencies (i.e., the percent of mercury removed from the flue gas) for the lowest sorbent injection rates, and with relatively less variability

(“FF” in Fig. 1). ACI upstream of an ESP at sites burning high sulfur (> 3.5%) coal (“ESP/Hi S”, Fig. 1) achieves removal efficiencies generally between 5 and 25%. Under some circumstances, the variability in performance can be quite large: Mercury removal efficiencies for ACI into an ESP range from less than 10% to greater than 90% for CFPPs burning low-sulfur, sub-bituminous Powder River Basin coals and no supplemental SO₃ injection (“ESP/PRB”, Fig. 1). SO₃ is a commonly used conditioning agent to improve fly ash removal in an ESP. Performance bands for several other combinations of site characteristics and coal type are typically presented, in addition to those schematically illustrated in Fig. 1.

Legal challenges to the Clean Air Mercury Rule (CAMR) have had implications for these uncertainties in ACI performance. Originally issued by the U.S. EPA in 2005, CAMR called for 50% reduction in mercury emissions by 2010 and nearly 70% reduction by 2018, making the U.S. the first country to regulate mercury emissions from CFPPs. The 2010 CAMR target, in particular, was significant because it provided CFPPs a pathway to regulatory compliance through so-called “co-benefits” [2], reductions in mercury emissions achieved collaterally during the control of other regulated pollutants such as NO_x (via selective catalytic reduction, SCR) and SO_x (via wet flue gas desulfurization, WFGD). WFGD is highly effective at removing the oxidized form (Hg²⁺) of mercury in the flue gas, routinely achieving > 70%–80% removal of Hg²⁺. Because the relative proportions of oxidized (Hg²⁺) and elemental (Hg⁰) mercury can vary widely, the corresponding reductions in total gaseous mercury

($\text{Hg}^0 + \text{Hg}^{2+}$) achieved by WFGD vary (see review by Pavlish et. al. [3]). SCR catalysts have shown evidence of oxidizing Hg^0 to Hg^{2+} , thereby facilitating total mercury removal in a downstream WFGD process. Hg^0 oxidation in SCRs appears to vary significantly as a result of the interfering effects of other flue gas constituents and fly ash [3,4]. Given the mercury reductions achievable through co-benefits, the CAMR target of 50% reductions by 2010 could conceivably have been achieved without ACI at some sites, and with limited ACI at others. With little or no use of ACI required to achieve CAMR-mandated targets by 2010, the uncertainties in ACI performance evident in Fig. 1 could be considered problematic, though perhaps not urgently so.

Fig. 1 Schematic representation of accumulated DOE-NETL



full-scale activated carbon injection (ACI) test results upstream of a fabric filter (FF) or electrostatic precipitator (ESP)

However, a unanimous ruling in *State of New Jersey vs. U.S. EPA* by a three-judge panel of the D.C. Circuit Court in February 2008 invalidated CAMR. The ruling essentially concluded that in implementing CAMR, U.S. EPA had, without justification, supplanted the authority of the Clean Air Act (CAA). The Clean Air Act requires the use of maximum achievable control technology (MACT) for reducing mercury emissions, as opposed to the passive control associated with the co-benefits-based, short-term targets of CAMR. Given the court's ruling, it will be difficult to craft a replacement mercury rule that differs from CAA while not contravening it. Thus, short of the U.S. Congress expressly legislating control of CFPP mercury emissions, future CFPP mercury emissions targets will likely be more aggressive than CAMR. In addition, at the time of the court's decision, 25 individual states had, or were considering, greater emissions reductions and/or more rapid time tables than existed in CAMR [5]. Although the state and federal regulatory landscapes continue to evolve, there is growing momentum for mercury emissions reductions that exceed those achievable through co-benefits. Meeting these targets will necessitate an increased reliance on ACI in the short-term.

The performance uncertainties evident in Fig. 1 become increasingly important with the growth in overall ACI usage and its contribution to total mercury removal. Rather than pursuing additional full-scale ACI testing to better understand the causes of these uncertainties, a more cost-effective strategy would be to develop a fundamental model of mercury capture during ACI, a model whose results could be validated against the extensive, existing collection of full-scale ACI results. The present investigation pursues this objective by validating recently developed models of mercury capture within ESPs using select full-scale ACI results at CFPPs employing ESPs. To our knowledge, this represents the first validated, fundamental model of mercury capture within an ESP. Not only will such validated models help elucidate and reduce the demonstrated uncertainty in ACI performance, but the results of such comparisons will enable efficient and effective ACI usage both domestically and abroad, particularly in developing countries. Reducing the need for full-scale, site-specific demonstrations of ACI lowers the economic barrier for developing countries to implement mercury emissions control technologies, thereby encouraging global mercury reductions. With recent estimates suggesting between one-fifth and one-half of mercury deposition on U.S. soil originates outside of the U.S. [6,7], global mercury reductions may be as important as domestic reductions with respect to reducing mercury exposures, regardless of location.

2 METHODOLOGY

The model of mercury capture within an ESP has been described in detail elsewhere [8-12], and therefore will only be briefly summarized here. The algorithm combines a particle charging and electrostatic drift analysis with a lumped capacitance mass transfer analysis between the flue gas and the suspended sorbent particles flowing within an ESP. The flue gas flow rate and the injection rate used for ACI yield an initial powdered sorbent mass loading in the flue gas entering the ESP. With this initial mass loading and a specified initial particle size distribution of the powdered sorbent, the algorithm obtains the instantaneous, cumulative gas-particle mass transfer rate by numerically integrating over the particle size distribution as the sorbent mass loading decreases and particle size distribution changes due to the electrostatic precipitation process. Integrating this instantaneous mass transfer rate forward in time yields the total mercury adsorbed (ΔM_{Hg} , Eq. (1)) after time interval τ .

$$\Delta M_{\text{Hg}} = \int_0^{\tau} \int_0^{\infty} \bar{h}_m(d_p) ND_p(d_p, t) \Delta V \cdot 4\pi \left(\frac{d_p}{2}\right)^2 \rho (C_v(t) - C_p(t)) d(d_p) dt \quad (1)$$

In Eq. (1), τ is the elapsed time considered for mercury adsorption by suspended sorbent particles, nominally equal to the characteristic flow time through the ESP (based on flue gas velocity and ESP depth). \bar{h}_m is the mean convective mass transfer coefficient for flow over a spherical sorbent particle of diameter d_p , ND_p is the number density of sorbent particles

of diameter d_p , ΔV is the control volume of flue gas within which the sorbent particles are suspended, ρ is the bulk density of the flue gas, C_V is the time-dependent concentration of mercury in the flue gas far removed from the particle, and C_p is the time-dependent gas-phase concentration of mercury adjacent to the particle surface, which is assumed to be in equilibrium with the solid-phase mercury concentration at the particle surface.

Although fly ash is known to have varying adsorption capacities for mercury [13,14], for simplicity, the present algorithm does not address fly ash adsorption of gas-phase mercury. The comparisons between the present algorithm and full-scale ACI results are limited to the additional mercury capture observed to occur across an ESP during ACI. Our previous analysis [8] concluded that even under idealized conditions, wall boundary mass transfer of gas-phase mercury to the ESP plate electrodes is slow, contributing a relatively small portion of the total mercury removal within typically sized ESPs; the dilution of the powdered sorbent on the ESP plate electrodes by the much larger ($\sim O(10^2)$) amounts of fly ash further diminishes the contribution of this removal mechanism.

The model, as described previously [8-12], employs the following assumptions:

1. No mercury adsorption by native fly ash;
2. No mercury adsorption by internal ESP surfaces;
3. Powdered sorbent is uniformly distributed throughout flue gas at ESP inlet;
4. Powdered sorbent mass concentration (g/m^3) varies only in the streamwise direction within the ESP;
5. All particles attain their theoretical maximum particle charge;
6. Fixed value of electric field voltage (54 kV).

The algorithm also employs additional assumptions regarding particle dielectric constant (very large), particle sphericity (perfect), flue gas pressure (atmospheric) and thermodynamic properties (ideal), and particle losses due to agglomeration, and rapping reentrainment and sneaking for the ESP (neglected). For all model results, the algorithm uses sorbent physical properties equal to those of NORIT Hg powdered activated carbon (PAC), primarily because of the many full-scale tests in which it has been used. In addition, and unlike other sorbent manufacturers, NORIT has made the detailed particle size distribution for this product readily available, which we have shown previously [10] has a strong influence on in-flight mercury capture. Fig. 1 shows the measured particle size distribution of the NORIT Hg PAC and the two curve fits (above and below $35 \mu\text{m}$) used to represent it in the model. Because flue gas composition is known to affect the rate and capacity of any sorbent to adsorb mercury, a lumped capacitance-mass transfer model of in-flight mercury capture would require some measure of the mercury adsorption capacity of a given sorbent at a particular site. Several of the early full-scale tests reported fixed bed equilibrium adsorption capacity for the NORIT PAC; however, subsequent full-scale tests eliminated this measure,

for reasons and with implications that will be discussed. In the absence of site-specific mercury adsorption capacity measurements for the NORIT Hg sorbent, estimates are used for the equilibrium adsorption capacity based on coal rank, an approach whose results and implications also will be discussed.

A collection of eleven full-scale tests of sorbent injection into cold-side ESPs using NORIT Hg sorbent constitute the field data against which the model results are compared: Six DOE-NETL-sponsored tests (Monroe 4, Leland Olds, Miami Fort 6, Brayton, Pleasant Prairie (PPPP), Meramec 2) and five proprietary, privately funded tests referred to here as Plants A through E. Table 1 presents a number of key parameters from each test program at each site. For DOE-NETL tests, many of the parameters can be found in the quarterly and final reports associated with each test program. In some instances, missing parameters were deduced from the available information (e.g., obtaining mean flue gas velocity from ESP geometry and design ESP specific collection area, SCA) or gleaned from diagrams and blueprints requested from the site operators.

3 RESULTS

Figs. 3 to 5 present comparisons between the model results and the full-scale ACI results at the eleven sites. Of the eleven full-scale ACI results, two – those from Brayton and Pleasant Prairie – provide on-site measurements of equilibrium mercury adsorption capacity of the NORIT Hg powdered activated carbon, using a fixed sorbent bed applied to a slipstream of the local flue gas. The present model requires as input a value for the equilibrium adsorption capacity of the sorbent, which determines the rate at which each sorbent particle approaches saturation during mercury adsorption, which in turn determines the rate at which the gas-phase mercury concentration at the particle surface ($C_p(t)$) approaches the far-field value ($C_V(t)$) (see Eq. 1). In the absence of measured, site-specific equilibrium mercury adsorption capacity at the other nine sites, a rough assumption was made that sites burning similar coals would exhibit similar equilibrium mercury adsorption capacities for the same sorbent. Although mercury adsorption kinetics are clearly much more complex than this assumption implies, it permits validation of the model against nine sites rather than two, and in its imprecision provides an opportunity to assess the degree to which each site's performance deviates from the ideal, mass-transfer-limited result.

Fig. 3 presents four comparisons of model results against full-scale ACI results at Leland Olds, Miami Fort 6, Brayton, and Plant C. Of these four, equilibrium mercury adsorption capacity was measured only at the Brayton site; model results for Leland Olds, Miami Fort 6, and Plant C adopt the Brayton value. Of the four sites, three burn bituminous coal, with Leland Olds burning North Dakota lignite. The agreement in all four cases ranges from good to excellent, with excellent agreement most often occurring at lower sorbent injection rates. Because the model represents a best case, mass-transfer-limited scenario, model results would be expected to form an upper performance limit, which is true in all four

cases. If other removal mechanisms were to play a significant role in mercury capture within an ESP (e.g., adsorption onto

internal surfaces such as plate electrodes), the expectation would be that some full-scale ACI results would significantly

Table 1 Selected Parameters of Modeled Full-Scale Sorbent Injection Tests

	Monroe 4	Leland Olds	Miami Fort 6	Brayton	PPPP	Meramec 2	Plant A	Plant B	Plant C	Plant D	Plant E
SCA [ft ² /kacfm]	285	320	353	403	468	320	173	144	328	299	234
Electrode length [ft]	35.9	36	46.5	54	36	49.3	21	18	12	36	36
Electrode spacing [in]	9	9	9	12	9	12	11	11	11	12	12
Gas temperature [°F]	260	375	284	280	280	320	310	300	275	300	270
Gas velocity [ft/s]	5.6	5	5.9	4.5	3.4	5.1	4.4	4.4	2.4	3.9	5.2
Inlet Hg concentration [ppb]	7.5	8.5	16	0.4	14.7	11	4	2.6	8-20	4.1	3
Coal Rank	PRB/Bit.	NDLig	E. Bit.	E. Bit.	PRB	PRB	E. Bit	E. Bit	E. Bit	PRB/Bit.	Bit.

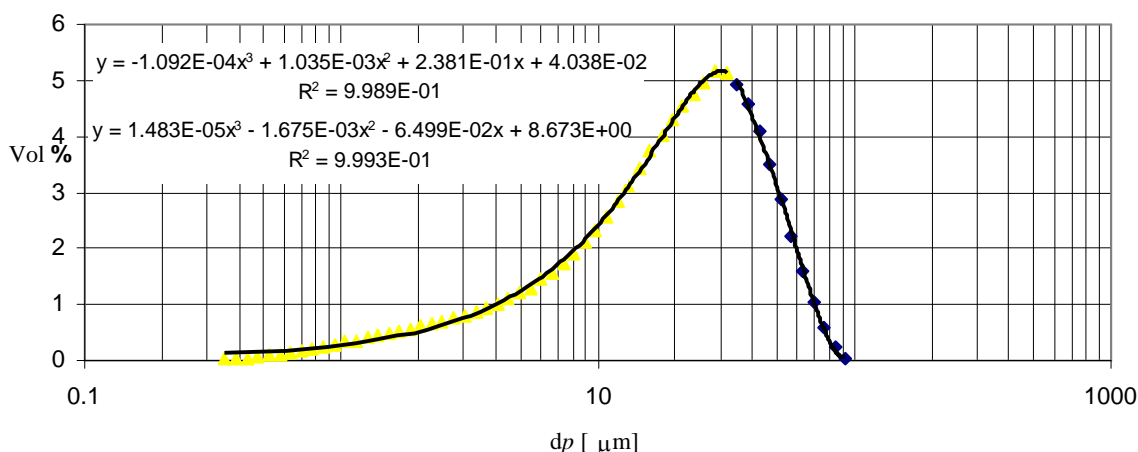


Fig. 2 Measured NORIT Hg particle size distribution, curve fits

exceed the model predictions; this is not the case in any of the comparisons in Fig. 3 or any of the results for the eleven sites.

The results comparison for the Brayton site should theoretically offer the highest fidelity of the four sites in Fig. 3 because of the availability of site-specific equilibrium mercury adsorption capacity measurements for use in the model. The Brayton comparison shows full-scale ACI results (symbols) compared against two model results (lines) representing the two different values of equilibrium adsorption capacity measured at the site. By using the commonly accepted method of directing a slipstream of flue gas through a fixed bed of sorbent, investigators at Brayton found [15] that the equilibrium mercury adsorption capacity of NORIT Hg in the Brayton flue gas fell from 4314 μg/g without SO₃ injection to 1380 μg/g with SO₃ injection. At the time of the Brayton testing (2002), such impacts on sorbent capacity due to SO₃ interference were relatively unknown. Since then, further fixed bed tests have confirmed the reduced equilibrium mercury adsorption capacity of powdered activated carbon in the presence of elevated SO₃ concentrations [16,17] and the resultant negative impacts on full-scale ACI performance during SO₃ injection [18,19].

Interestingly, despite the measured reduction in fixed bed adsorption capacity at Brayton, full-scale ACI performance there showed little response to SO₃ injection. At a PAC injection rate of 10 lbs/MMacf, mercury removal efficiency across the ESP with SO₃ injection (70-73%) was essentially unchanged from its value without SO₃ injection (71%) [15]. At a PAC injection rate of 20 lbs/MMacf, mercury removal efficiency across the ESP dropped from 93% without SO₃ injection to 90% with SO₃ injection [15]. While these data do not show the decrease in full-scale ACI performance that was expected to accompany the large decrease in equilibrium mercury adsorption capacity, the associated model results do. In Fig.3 the model results for the higher capacity (SO₃ injection off) and lower capacity (SO₃ injection on) conditions bracket the full-scale ACI performance data from above and below. Given the more recent full-scale ACI results [18,19] showing a strong, negative impact of SO₃ injection, when combined with the well-known impacts of SO₃ on equilibrium mercury adsorption capacity, it is difficult not to conclude that the effects of SO₃ on full-scale ACI performance are not accurately reflected in the full-scale Brayton data. One possible reason may lie in the physical

layout of the Brayton tests. The Brayton facility operates with two ESPs in series, with SO_3 injection located upstream of both units. However, during the ACI tests, PAC injection was located in between the two ESPs. Given the concentrations of fly ash entering the first ESP and the potential for electrohydrodynamic mixing caused by the strong electric fields, it is possible that much of the injected SO_3 was adsorbed onto fly ash before the point of PAC injection. This would lead to relatively lower SO_3 concentrations at the point of PAC injection and beyond and correspondingly decreased potential for SO_3 interference effects on mercury adsorption.

The model predictions agree quite well with the field data for Leland Olds, Plant C, and Miami Fort 6 sites.

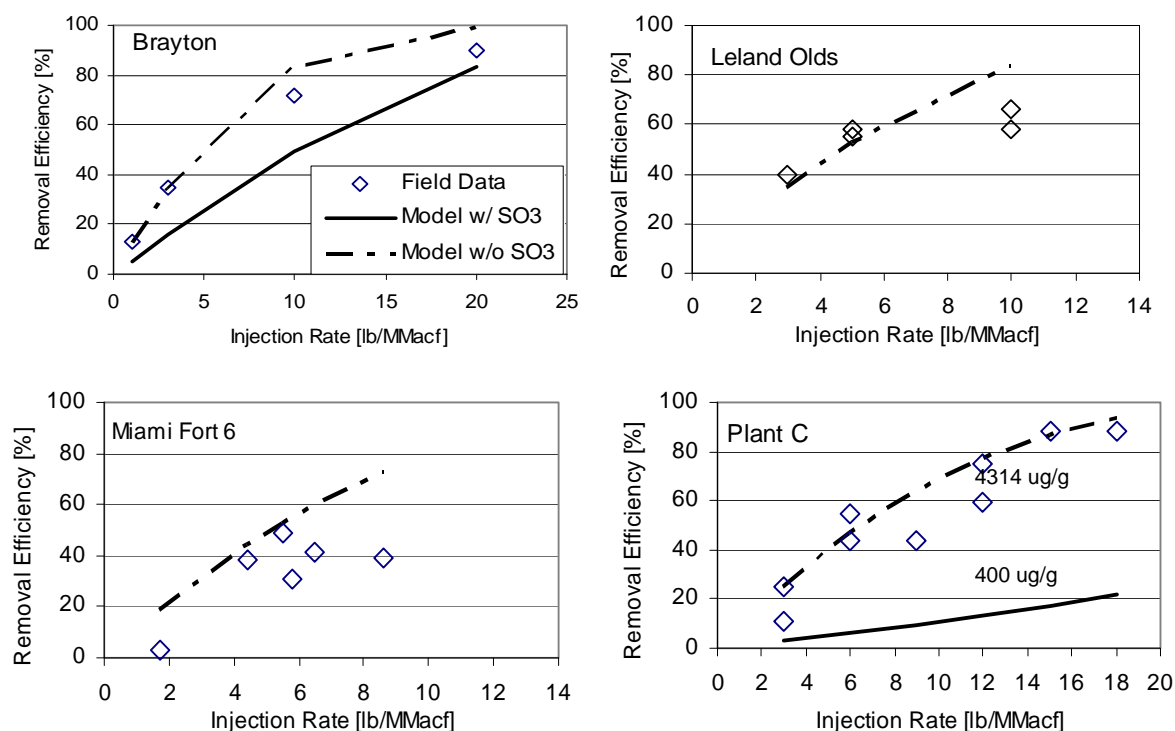


Fig. 3 Comparisons of model results to full-scale sorbent injection test data taken at Brayton, Leland Olds, Miami Fort 6, and Plant C. Lines represent model predictions; open symbols represent field data. Two model results for Plant C represent assumed equilibrium mercury adsorption capacities of 400 $\mu\text{g/g}$ (solid) and 4314 $\mu\text{g/g}$ (dashed)

The comparison results for Plant C (Fig. 3) offer further proof that the mass-transfer-limited model represents an upper limit to ACI performance, which is particularly evident given the scatter in the full-scale ACI data for this site. The agreement between the model and full-scale ACI data for Plant C is also over a much wider range of sorbent injection rates (up to 18 lb/MMacf) than was the case for Miami Fort 6 or Leland Olds. The Plant C data also illustrate the effect of the decision to discontinue on-site measurement of fixed bed equilibrium mercury adsorption capacity as a part of full-scale ACI tests.

On-site measurement of equilibrium mercury adsorption capacity was discontinued after the Brayton and Pleasant Prairie (presented in Fig. 5) full-scale tests. The decision was based on an analysis of a mass median diameter-sized PAC particle within an ESP, comparing the diffusive mass transfer rate to the particle surface to the characteristic retention time of

Duplicate full-scale data points in the Leland Olds and Plant C results provide an indication of the variability and/or uncertainty in the full-scale ACI performance measurements and diminish the implications of the few data points that appear to exceed the model predictions (lines) in this investigation. The Leland Olds comparison results suggest that the agreement between the model and the ACI data at low sorbent injection rates (3 and 5 lb/MMacf) becomes worse at higher injection rates (10 lb/MMacf), a phenomenon that is also evident in the Miami Fort 6 comparison results and which will be explored later in more details.

the flue gas within the ESP. The analysis concluded that a mass median-sized particle could utilize no more than 150 $\mu\text{g/g}$ of its mercury adsorption capacity within a typical ESP, a quantity referred to as the “threshold capacity” in the Brayton [15] and Pleasant Prairie [20] project reports. Because most sorbents have at least an order of magnitude greater equilibrium mercury adsorption capacity, the analysis concluded that virtually all sorbents have sufficient capacity, but are limited mostly by insufficient residence time in the ESP. This conclusion led to the decision to discontinue on-site measurement of equilibrium mercury adsorption capacity during full-scale ACI tests.

The Plant C comparisons in Fig. 3 show two model results representing different assumed equilibrium mercury adsorption capacities: a value of 400 $\mu\text{g/g}$ (solid, 2.7 times the “threshold capacity” value) and a value of 4314 $\mu\text{g/g}$ (dashed, equal to the measured capacity at Brayton, also burning

bituminous coal). It is clear from Fig. 3 that the threshold capacity of 150 $\mu\text{g/g}$ would grossly underpredict mercury removal efficiency, given that even a value of 400 $\mu\text{g/g}$ results in a large degree of underprediction. By comparison, adopting the Brayton site equilibrium capacity of 4314 $\mu\text{g/g}$ produces very good agreement between the model results and the Plant C full-scale ACI performance data. The analysis used to evaluate the threshold capacity likely can be faulted on more than one basis. A mass median diameter-sized particle fails to capture the role played by fine particles, which undergo rapid mass transfer and slow precipitation within an ESP. Also, the analysis assumes diffusive mass transfer to the particle surface and does not consider the charge-driven relative motion between a particle and the flue gas and the convective mass transfer enhancement that result.

Fig. 4 presents comparisons between model results and field data for Plant A, Plant D, and Monroe 4. The agreement is excellent between the model results and the full-scale ACI data for Monroe 4. However, the agreement between the model and the full-scale results for the proprietary sites is less good. For Plant D, the discrepancy may reflect the effects of more complex flue gas chemistry and adsorption kinetics that are not captured in the present model. The Plant D testing program was designed to examine the effect on mercury capture of blending different coal types. As Fig. 4 shows, for sub-bituminous PRB/bituminous mixtures, increasing the bituminous percentage from 20% to 40% produced a modest increase in mercury removal efficiency at most sorbent injection rates. No on-site measurements of equilibrium mercury capacity were taken at Plant D for the different coal blends. As a result, the model uses values representing 100% sub-bituminous PRB (8823 $\mu\text{g/g}$) and 100% bituminous (4314 $\mu\text{g/g}$), values measured during the Pleasant Prairie and Brayton full-scale tests, respectively, and which would be expected to bracket the full-scale results for the sub-bituminous/bituminous coal blends. While these values are clearly not an ideal representation of the Plant D tests, it is notable that results obtained using these values exhibit a somewhat similar trend as the full-scale data, with higher capacities leading to higher mercury removal efficiencies. Other factors that may have influenced the full-scale data include poor sorbent mixing and distribution in the flue gas. Fig. 4 also presents comparisons for Plant A. This comparison features a clear and pronounced divergence between the model results and the field data with increasing sorbent injection rate, similar to Leland Olds (Fig. 3), where the full-scale ACI data appears to reach a performance plateau. That the mass transfer-based model results are consistently higher than the field data supports the assertion that mass transfer-limited analyses represent the upper limit of adsorption performance in these situations. The nature of the divergence and performance plateau has been attributed to the injected PAC adsorbing chlorine-containing species needed for the oxidation of Hg^0 to HgCl_2 , the much more condensable and easily removed form of mercury. However, as far as we are aware, no conclusive evidence or fundamental analysis has

been presented that confirms this hypothesis. It is also possible that, as sorbent injection rate increases, so too does the rate of agglomeration between PAC particles. Because the model assumes a fixed particle size distribution, increased agglomeration would increase the mean particle size and decrease the overall mass transfer rate to the sorbent particles in the full-scale tests. The available full-scale ACI data is insufficient to conclusively differentiate between the two potential causes of the divergence and performance plateau. However, it should be noted that for the three sites exhibiting varying degrees of performance plateau, their coal chlorine concentrations (91 mg/kg at Leland Olds, 150 mg/kg-450 mg/kg at Plant A, and 1000 mg/kg at Miami Fort 6) are substantially similar to those of sites exhibiting no performance plateau (150 mg/kg-642 mg/kg at Plant C and 100 mg/kg and 500 mg/kg at Monroe 4). Thus, on this basis, it is difficult to argue that low concentrations of chlorine-containing species are solely responsible for the performance plateau phenomenon. A separate investigation is ongoing to assess the potential for sorbent agglomeration during feeding for a subset of these full-scale tests, based on detailed knowledge of their sorbent feeding systems.

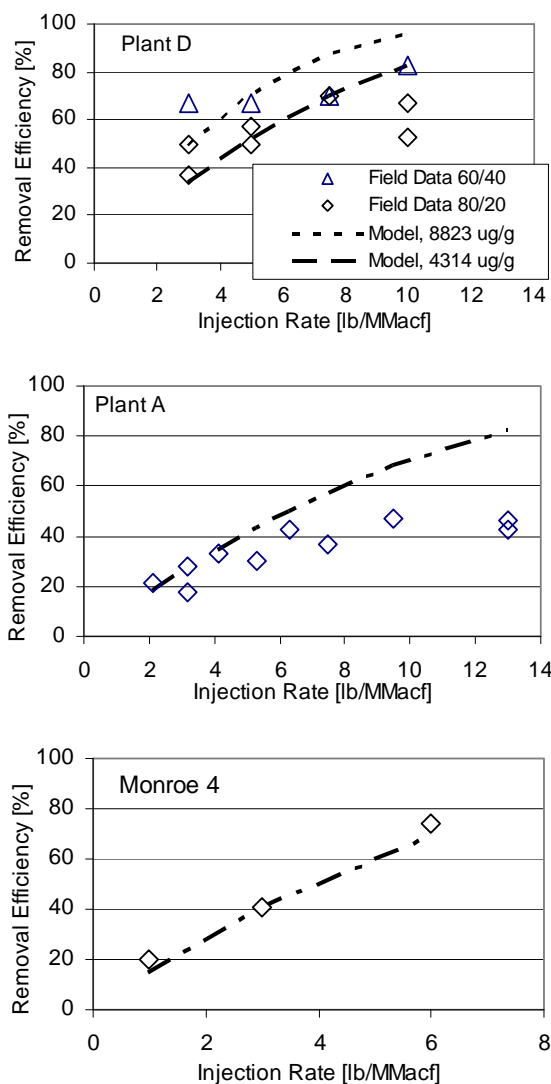


Fig. 4 Comparisons of model results to full-scale sorbent injection test data taken at Plant D, Plant A, and Monroe 4. Dashed lines represent model predictions; open symbols represent field data

Fig. 5 presents comparison results for Meramec 2, Pleasant Prairie, Plant B, and Plant E, all cases where agreement was marginal to poor. In the case of Meramec 2, much of the discrepancy between the model results and the full-scale data can be traced to the variability in the baseline mercury capture by the native fly ash, which is not accounted

for in the model. As shown in Fig. 5, native capture of mercury by fly ash alone at Meramec 2 (i.e., measured mercury removal efficiencies at 0 lb/MMacf injection rate of PAC) varied from 13% to 53%. At low sorbent injection rates, this variability is of the same scale as the difference between the model results and the measured mercury removal efficiencies. At high sorbent injection rates, a divergence between the model and full-scale results and a plateau in full-scale performance are evident, similar to that discussed above for Plant A (Fig. 4).

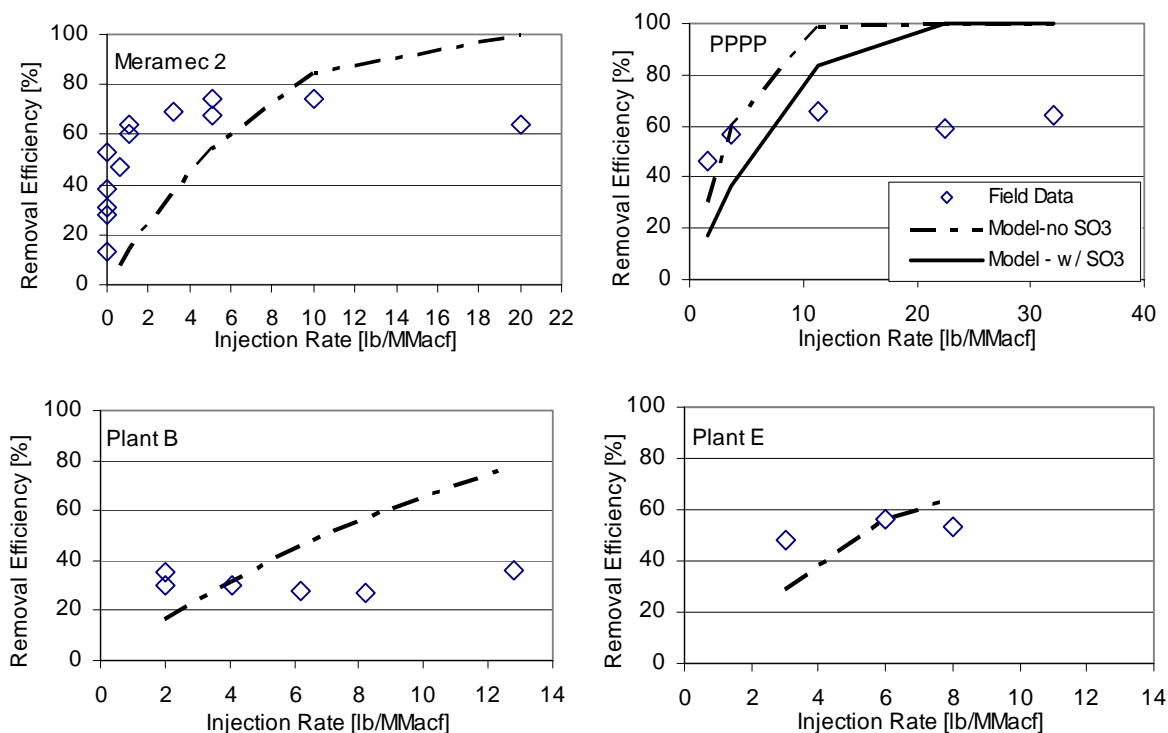


Fig. 5 Comparisons of model results and full-scale ACI test results for Meramec 2, Pleasant Prairie, and proprietary Plants B and E. Dashed lines represent model predictions; open symbols represent field data

The results comparison for Pleasant Prairie (PPPP, Fig. 5) also show increasing divergence between full-scale ACI results and model results and a plateau in full-scale performance with increasing sorbent injection rate. The poor agreement between the model and the full-scale results for PPPP is not entirely surprising, as the anomalous nature of the field data, particularly the performance plateau at very high sorbent injection rates (> 30 lb/MMacf), has been widely reported. The PPPP performance plateau is often attributed to the same phenomenon of low chlorine levels (< 100 mg/kg) discussed previously. The full-scale ACI data for both Plant B and Plant E (Fig. 5) show little or no response to changes in sorbent injection rates at all levels. Engineers at both Plant B and Plant E cited poor sorbent dispersion as a possible cause.

ACKNOWLEDGEMENTS

The author wishes to thank Ed Morris (We Energies), Tom Hart (Ameren) and the many other industry personnel who provided detailed ESP specifications for their sites, and without which this work would not have been possible.

REFERENCES

1. Feeley, T.J., Jones, A.P. An Update on DOE/ NETL's Mercury Control Technology Field Testing Program. White paper available at <http://www.netl.doe.gov/technologies/coalpower/ewr/mercury/pubs/netl%20Hg%20program%20white%20paper%20FINAL%20Jan2008.pdf> (2008).
2. Srivastava, R.K., Hutson, N., Martin, B., Princiotta, F., Staudt, J. Control of Mercury Emissions from Coal-Fired Electric Utility Boilers: An Overview of the Status of Mercury Control Technologies. *Environ. Sci. Technol.*, 2006, 40: 1385-1393.
3. Pavlish, J.H., Sondreal, E.A., Mann, M.D., Olson, E.S., Galbreath, K.C., Laudal, D.L., Benson, S.A. Status review of mercury control options for coal-fired power plants. *Fuel Proc. Technol.*, 2003, 82: 89-165.
4. Lee, C.W., Serre, S.D., Zhao, Y., Lee, S.J., Hastings, T.W. Mercury Oxidation Promoted by a Selective Catalytic Reduction Catalyst under Simulated Powder

- River Basin Coal Combustion Conditions. *J. Air Waste Manage. Assoc.*, 2008, 58: 484-493.
5. Becker, W. States' Programs to Control Mercury from Coal-fired Power Plants. Presentation at Virginia Mercury Symposium, November 29, 2007.
 6. Levin, L. New Perspectives on Mercury in the Human Environment. Written remarks delivered to Committee on Environment and Public Works, United States Senate, July 29, 2003.
 7. Jaffe, D, Strode, S. Sources, fate and transport of atmospheric mercury from Asia. *Environ. Chem.*, 2008, 5: 121-126.
 8. Clack, H. L. Mass transfer within electrostatic precipitators: trace gas adsorption by sorbent-covered plate electrodes. *J. Air Waste Manage. Assoc.*, 2006, 56: 759-766.
 9. Clack, H. L. Mass transfer within electrostatic precipitators: in-flight adsorption of mercury by charged suspended particulates. *Environ. Sci. Technol.*, 2006, 40: 3617-3622.
 10. Clack, H. L. Particle size distribution effects on gas-particle mass transfer within electrostatic precipitators. *Environ. Sci. Technol.*, 2006, 40: 3929-3933.
 11. Clack, H.L. Bimodal Fly Ash Distributions and Their Influence on Gas-Particle Mass Transfer During Electrostatic Precipitation. *Fuel Proc. Technol.*, 2006, 87: 987-996.
 12. Scala, F., Clack, H. L. Mercury emissions from coal combustion: Modeling and comparison of Hg capture in a fabric filter versus an electrostatic precipitator. *J. Haz. Materials*, 2008, 152: 616-623.
 13. Senior, C.L., Johnson, S.A. Impact of carbon-in-ash on mercury removal across particulate control devices in coal-fired power plants. *Energy Fuels*, 2005, 19: 859-863.
 14. Lu, Y., Rostam-Abadi, M., Chang, R., Richardson, C., Paradis, J. Characteristics of Fly Ashes from Full-scale Coal-fired Power Plants and Their Relationship to Mercury Adsorption. *Energy Fuels*, 2007, 21: 2112-2120.
 15. ADA Environmental Solutions. Brayton Point Generating Station Unit 1-Sorbent Injection into a Cold-side ESP for Mercury Control. Final Report, U.S. Dept. of Energy, Cooperative Agreement No. DE-FC26-00NT41005, March, 2005.
 16. Presto, A. A., Granite, E.J. Impact of Sulfur Oxides on Mercury Capture by Activated Carbon. *Environ. Sci. Technol.*, 2007, 41: 6579-6584.
 17. Presto, A. A., Granite, E.J. Further Investigation of the Impact of Sulfur Oxides on Mercury Capture by Activated Carbon. *Ind. Eng. Chem. Res.*, 2007, 46: 8273-8276.
 18. Sjostrum, S., Wilson, C., Bustard, J., Spitznogle, G., Toole, A., O'Palko, A., Chang, R. Full-scale evaluation of carbon injection for mercury control at a unit firing high sulfur coal. In Proceedings of the U.S. EPA - DOE - EPRI Combined Power Plant Air Pollutant Control Symposium: The MEGA Symposium (2006).
 19. Cushing, K.M., Heaphy, R.F., Jarvis, J., Wells, S., Berry, M.S., Irvin, N., Chang, R.L. Impact Of Flue Gas Characteristics And ESP Operating Variables On Mercury Removal And ESP Capture Of Activated Carbon. In Proceedings of Air Quality VI Conference, September 24-27, 2007, Crystal City, Virginia.
 20. ADA Environmental Solutions. Pleasant Prairie Power Plant Unit 2 - Sorbent Injection into a Cold-side ESP for Mercury Control. Final Report, U.S. Dept. of Energy, Cooperative Agreement No. DE-FC26-00NT41005, May, 2003.